ISSN 0021-3640, JETP Letters, 2011, Vol. 94, No. 3, pp. 171–176. © Pleiades Publishing, Inc., 2011.
Original Russian Text © A.Ya. Faenov, I.Yu. Skobelev, T.A. Pikuz, V.E. Fortov, A.S. Boldarev, V.A. Gasilov, L.M. Chen, L. Zhang, W.C. Yan, D.W. Yuan, J.Y. Mao, Z.H. Wang, J. Colgan, J. Abdallah Jr., 2011, published in Pis'ma v Zhurnal Eksperimental'noi i Teoreticheskoi Fiziki, 2011, Vol. 94, No. 3, pp. 187–193.

# Diagnostics of the Early Stage of the Heating of Clusters by a Femtosecond Laser Pulse from the Spectra of Hollow Ions

**A. Ya. Faenov[a, e, *], I. Yu. Skobelev[a], T. A. Pikuz[a, e], V. E. Fortov[a], A. S. Boldarev[b], V. A. Gasilov[b], L. M. Chen[c], L. Zhang[c], W. C. Yan[c], D. W. Yuan[c], J. Y. Mao[c], Z. H. Wang[c], J. Colgan[d], and J. Abdallah Jr.[d]**

[a] *Joint Institute for High Temperatures, Russian Academy of Sciences, ul. Izhorskaya 13/19, Moscow, 125412 Russia*
* *e-mail: anatolyf@hotmail.com*
[b] *Institute of Mathematical Modeling, Russian Academy of Sciences, Miusskaya pl. 4a, Moscow, 125047 Russia*
[c] *Institute of Physics, Chinese Academy of Sciences, Beijing, 100190 People's Republic of China*
[d] *Los Alamos National Laboratory, NM 87545 Los Alamos, USA*
[e] *Quantum Beam Science Directorate, Japan Atomic Energy Agency, 619-0215 Kyoto, Japan*

Received May 24, 2011

Differences between X-ray argon clusters excited at the laser-cluster and laser-droplet interactions have been analyzed. X-ray spectral methods have been proposed to determine the parameters of the appearing plasma at the early stages of its evolution. It has been shown that the spectra of hollow ions are the most informative in the first moments of the heating of a cluster, whereas the diagnostics of the late stages can be performed using the conventional lines of multicharged ions.

**DOI:** 10.1134/S0021364011150033

**1.** Studies of the interaction of intense laser pulses with cluster targets are of current interest. On one hand, these studies provide information on the fundamental properties of matter under extreme conditions. On the other hand, these studies make it possible to use new approaches to achieve a number of applied purposes, such as the initiation of nuclear reactions, the acceleration of electrons and heavy particles, and the creation of a bright X-ray source for biomedical and lithographic applications.

The use of cluster targets imposes constraints on the duration of a laser pulse. The interactions will obviously be efficient if a cluster is not completely destroyed during the pulse, i.e., the density of the cluster does not become lower than the critical value due to a Coulomb explosion. For all reasonable sizes of clusters, this condition means that the duration of the laser pulse should be in the femtosecond or subpicosecond range; i.e., only ultrashort laser pulses can efficiently interact with clusters.

However, even in this case, the cluster should not be too small, because the ultrashort laser pulse always involves a pre-pulse, usually with picosecond duration. The contrast of the laser pulse, i.e., the ratio of the power of laser radiation in the maximum of the femtosecond pulse to the power of the pre-pulse, is normally no larger than $10^4$–$10^6$ and even smaller without special measures. This means that, if the main pulse is fairly intense (experiments are usually performed at flux densities $q_{las} > 10^{17}$–$10^{18}$ W/cm$^2$), the flux density in the pre-pulse is no lower than $10^{13}$–$10^{14}$ W/cm$^2$ and is sufficient to destroy the cluster, even before the arrival of the main pulse. For the main pulse to interact with the dense core of the cluster, its size should be about 1 μm. The most interesting results have been obtained recently for clusters of this size (see, e.g., [1–14]).

FS laser pulses with a superhigh contrast of about $10^{10}$–$10^{11}$ have recently become available [15–22]. In this case, the laser pre-pulse does not destroy the cluster and the high interaction efficiency can be ensured for much smaller clusters. For example, if the duration of the pulse is 1 ps, the cluster size can be as small as 0.1 μm. Since the thickness of a skin layer for the wavelength of most widespread lasers is about this size, the use of not too large clusters makes it possible to study a quite different type of interaction, notably the interactions at which the entire bulk of the cluster, rather than its skin layer, is heated as a whole. This interaction is called the laser–cluster interaction, unlike the previously studied interaction, which is more correctly called the laser–droplet interaction. We emphasize that experiments with this process have only become possible due to the creation of femtosecond lasers with superhigh contrast.

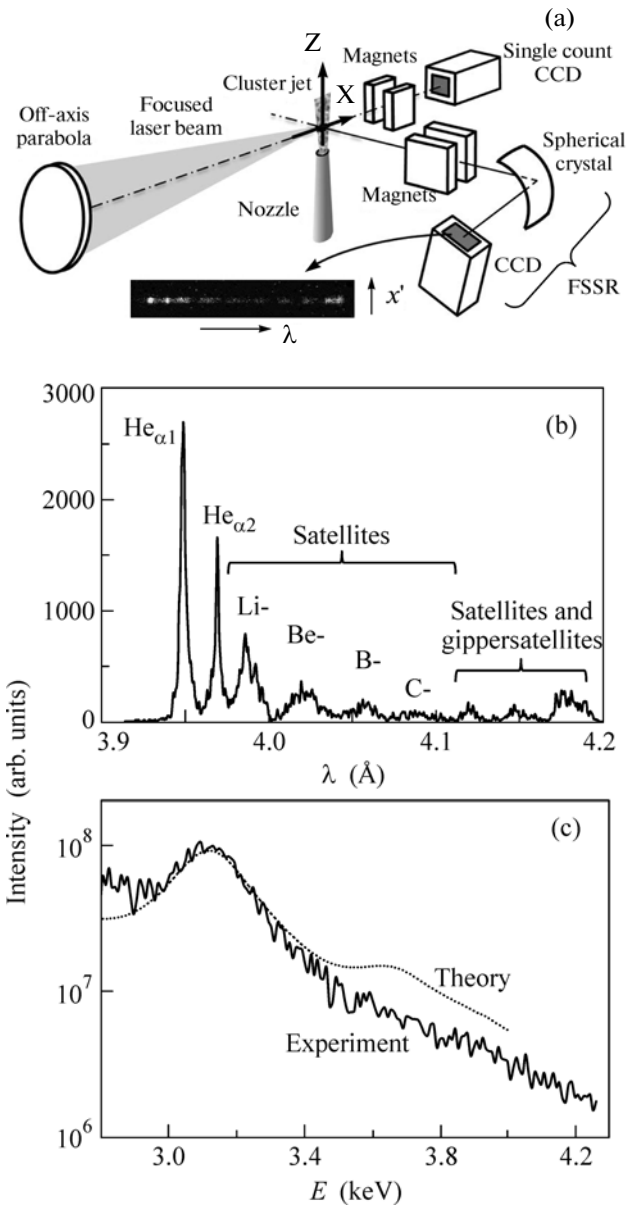


**Fig. 1.** (a) Layout of the experiment. (b) Typical densitogram of the spectrum of the argon plasma in the wavelength range 3.9–4.3 Å, which was detected by the FSSR spectrometer. (c) Broadband X-ray spectrum that was detected by a CCD in the single count mode.

The aim of this work is to examine this interaction. The performed experiments allow us to analyze the differences in the emission X-ray spectra of argon clusters excited at laser–cluster and laser–droplet interactions for the first time. X-ray spectral methods are proposed to determine the parameters of the appearing plasma at the early stages of its evolution. It is shown that, in the first moments of the heating of a cluster, the spectra of hollow ions are most informative, whereas the diagnostics of the late stages can be performed using the conventional lines of multicharged ions.

**2.** Experiments were carried out at the Xtreme Light III (XL–III) laser facility at the Institute of Physics, Chinese Academy of Sciences. A Ti: sapphire laser, which operated in the chirped scheme, generated linearly polarized pulsed radiation at a wavelength of 800 nm with an energy of up to 1 J and a duration of about 100 fs. The contrast of laser radiation at a scale of hundreds of picoseconds from the 100-fs main pulse was increased to $10^{10}$ by using the so-called OPCPA scheme [23]. This laser contrast is almost four orders of magnitude higher than the typical contrast of previously used laser facilities.

A laser beam was focused in a vacuum chamber by an off-axis parabolic mirror ($f$/2.0) onto a pulsed gas-cluster argon target (Fig. 1a). The size of the focal spot on the target in vacuum at the $1/e^2$ intensity level was about 7 μm and the laser energy flux density reached $q_{las} = 2.6 \times 10^{19}$ W/cm$^2$. To produce clusters, a conical nozzle 6 mm in length with the input and output holes with diameters of 1.0 and 2.0 mm, respectively, was used. A supersonic pulsed argon jet was produced at the output of the nozzle. The pressure of the gas supplied to the nozzle was optimized to increase the yield of clusters with a radius of $R_{cl} \sim 0.15$ μm. To this end, we performed calculations with software packages used to describe gas-dynamic processes in nozzles that form two-phase jets [24, 25]. According to the calculations, a cluster diameter of 0.3 μm and a maximum atomic density of $N_{Ar} \sim 1.5 \times 10^{20}$ cm$^{-3}$ at a distance of 1 mm from the nozzle edge are achieved at a gas pressure of 70 bar. The experiment indicated that the maximum X-ray emission was observed at this gas pressure.

X rays from the plasma produced at the interaction of laser radiation with argon clusters were detected by a focusing spectrometer with spatial resolution (FSSR) [26–28] based on a 10–20 quartz crystal ($2d \sim 4.9$ Å) bent over a spherical surface with a radius of $R =$ 150 mm (Fig. 1a). The spectrometer was used in the FSSR-1D regime in which the detector is placed on the Rowland circle and the spectral resolution is independent of the source size. The position of the spectrometer ensured the detection of spectra with the spatial resolution along the axis of the laser beam. The central wavelength was $\lambda_0 = 3.9$ Å. The spectral detection range was 3.7–4.25 Å. The distance from the focusing point of laser radiation to the center of the crystal was $a = 449.4$ mm. The spectral resolution of the spectrometer was no worse than ~3000 and the spatial resolution was $\delta x \sim 50$ μm. A DX-440 X-ray CCD camera with a pixel size of 13.5 μm was used as a detector. The sensitive area of the camera was protected from the visible and ultraviolet radiation by two layers of 1-μm polypropylene filter coated on both sides by a 0.2-μm aluminum film. Figure 1b shows the typical densitogram of the spectrum in the wavelength range 3.9–4.3 Å.

The X-ray spectrum in a wide energy range was measured by a 16-bit CCD that operated in the single

count mode and was placed at a distance of about 1.2 m from the plasma (Fig. 1a). The detector was screened by 30-μm Be and 12.5-μm Al filters in order to cut off low-energy photons. In order to deflect hot electrons accelerated in the laser plasma, an additional strong magnet was placed between the plasma and detector. Figure 1c shows a spectrum recorded by this instrument.

**3.** In our previous works [21, 29–31], the spectra of the argon plasma were studied in the laser–droplet interaction regime. It was found that various stages of the evolution of the produced plasma contribute to the observed time-integrated X-ray emission spectrum. The long-wavelength part of the spectrum shown in Fig. 1b is formed at the initial heating stage by the densest regions that are not strongly heated, whereas the short-wavelength part is formed by the less dense, hotter plasma at the much later stage. Since the size of clusters in those experiments was about 1 μm, i.e., was much larger than the thickness of the skin layer, the heating of the cluster was nonuniform. When its surface layer had been already heated to a high temperature and began to expand, the inner part still remained cold and immobile.

In the case under consideration, all parts of the cluster will be heated simultaneously and the plasma created at the heating stage will be much more uniform. Using the previously developed stationary kinetic model and the atomic constants calculated for argon ions [21], we can calculate the emission spectrum corresponding to this stage of the plasma evolution. Until the cluster does not noticeably expand (i.e., until time $\tau_{exp} \sim R_{cl}/v_{ion} \sim 150$ fs at a typical value of $v_{ion} \sim 10^8$ cm/s), its atomic density can be treated as constant $N_{Ar} = 2.1 \times 10^{22}$ cm$^{-3}$. In this case, the spectrum will depend on only one parameter, i.e., the electron temperature $T_e$ of the plasma, because its electron density (and the ionization degree) will be determined by the balance equations. According to the model proposed in [21], we include the 1% fraction of hot electrons with a mean energy of 7 keV into the kinetic equations. The spectra calculated for various temperatures in the range of 10–100 eV are shown in Fig. 2a.

The spectral range shown in Fig. 2a (see also Fig. 1b) includes three broad spectral structures with the average wavelengths of 4.11–4.13, 4.14–4.15, and 4.18–4.20 Å. Each of these structures can generally consist of a number of various spectral transitions both well known transitions ($K_\alpha$ lines and dielectronic satellites) and transitions the study of which has begun only recently (transitions in hollow ions or hypersatellites [15, 16, 21, 29–36]). The $K_{\alpha 1}$ (4.1918 Å) and $K_{\alpha 2}$ (4.1947 Å) lines of the neutral atom are in the right structure. This structure includes the *F*-like satellites $1s2s^22p^6$–$1s^22s^22p^5$. The central structure includes the *O*-like satellites $1s2s^22p^5$–$1s^22s^22p^4$, and the *N*-like satellites $1s2s^22p^4$–$1s^22s^22p^3$ enter into the left structure. In addition, the right, central, and left structures can include hypersatellites of the types

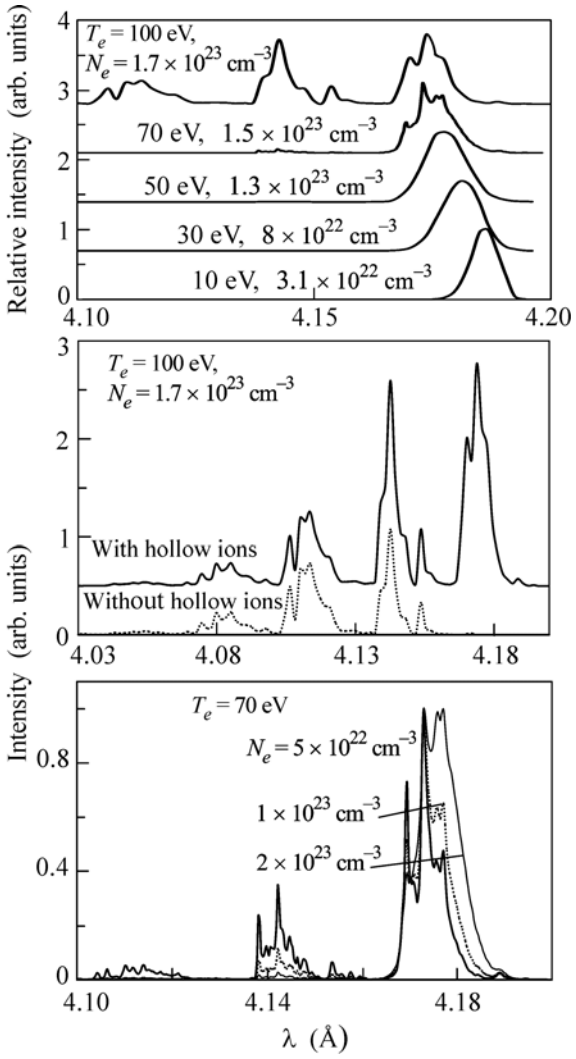


**Fig. 2.** (a) Emission spectra of the argon plasma that are calculated in the stationary kinetic model for various temperatures. (b) Contribution of transitions in hollow ions to the emission spectrum. (c) Spectra at a fixed temperature for various electron densities.

$$1s2s^22p^63s^k3p^m - 1s^22s^22p^53s^k3p^m,$$
$$1s2s^22p^53s^k3p^m - 1s^22s^22p^43s^k3p^m,$$
$$1s2s^22p^43s^k3p^m - 1s^22s^22p^33s^k3p^m,$$

respectively, which are transitions in *KL* hollow ions (for details, see [15, 16, 21, 29–36]).

It can be seen in Fig. 2a that an increase in the temperature of the plasma is accompanied by a noticeable change in the emission spectrum. This change for the right structure is mainly manifested in the shift of the position of its center of gravity, whereas the relative intensities of the central and left structures increase.

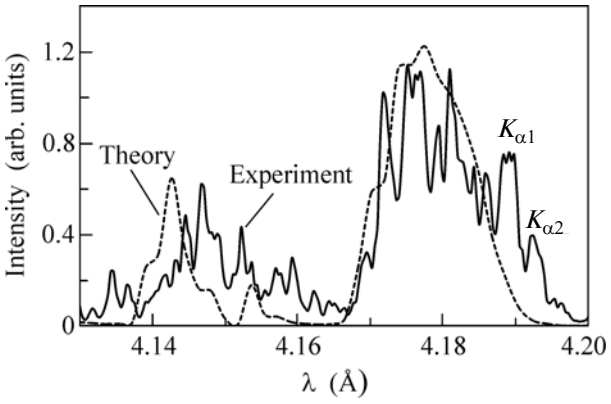


**Fig. 3.** Detected and calculated spectra for wavelength range 4.13–4.20 Å.

To determine the contribution to the emission spectrum from radiative transitions of various types, we perform calculations disregarding transitions in hollow ions. These calculations showed that, for low temperatures below 50 eV, the emission spectrum almost completely consists of lines of hollow ions. At a temperature of 100 eV, hollow ions completely determine the right spectral structure, make an approximately 50% contribution to the intensity of the central structure, and are hardly manifested in the left structure (see Fig. 2b). Thus, the emission of clusters at low temperatures is almost completely determined by transitions in hollow ions; moreover, their contribution in the longest-wavelength part of the spectrum under consideration is noticeable even for the high-temperature plasma.

Figure 2c shows the emission spectra at a fixed temperature for various plasma densities. It can be seen that an increase in the density leads to a decrease in the plasma ionization degree. This is obvious because an increase in the density is accompanied by a fast increase in the collisional recombination rate and by a transition from the coronal ionization equilibrium to the Saha equilibrium. Note that the effect of an increase in $N_e$ on the emission spectrum is similar to that of a decrease in $T_e$ because, in both cases, the plasma ionization degree decreases.

The spectra of hollow ions can be used for the diagnostics of the heating of clusters at the stage of the action of the main laser pulse. If spectra are recorded without time resolution, the observed spectrum will be naturally determined by a continuous set of temperatures, rather than one temperature. It can be assumed that the temperature in the heating process increases monotonically according to an increase in the absorbed laser energy to a certain maximum value $T_{max}$ and the integral of emittance over time, which will depend on $T_{max}$, can be calculated. After that, we can try to obtain the best description of the long-wavelength part of the observed spectrum by varying $T_{max}$. The best agreement for this experiment was obtained with $T_{max}$ = 100 eV (Fig. 3). Note that the MUTA approximation used within the software packages [37–41] results in a small discrepancy between the calculated and measured spectra. In this case, the most important characteristic is the integral emittance of the plasma in each of the spectral structures under consideration.

It is interesting to compare this result with the previous result for larger clusters. Recall that the long-wavelength part of the spectrum is well simulated in [21] by a set of much lower temperatures (10–30 eV). This indicates that, in the case of the laser–droplet interaction, the dense core of the cluster remains unheated, even after the end of the heating pulse and the average temperature at this stage is noticeably lower. This is also confirmed by the very high intensity of the $K_\alpha$ lines detected in the experiment reported in [21], because hot electrons and neutral argon atoms should be simultaneously present for the emission of these lines. In the case of the laser–cluster interaction, hot electrons appear simultaneously with the fast initial ionization of argon atoms by the optical laser field in almost the entire volume of the cluster. In other words, to the time of the appearance of hot electrons, all argon atoms are ionized and a $K_\alpha$ line cannot be emitted. A low-intensity $K_\alpha$ line is present in the spectra observed in this work for two reasons. First, the size of the cluster is slightly larger than the thickness of the skin layer (i.e., this is not the case of the pure laser–cluster interaction). Second, the $K_\alpha$ line was emitted by cold clusters located near the focal spot, which were bombarded by fast electrons generated in the central region of the focal spot.

It was shown in [21] that the short-wavelength part of the spectrum shown in Fig. 1b is determined by the times at which clusters have already expanded and formed a quite uniform plasma channel. The plasma parameters at this stage of its evolution can be determined from this part of the spectrum. As in the preceding case, the time dependence of the plasma parameters should be taken into account and the time-integral spectrum should be simulated by the sum of at least several points in the density and temperature. Recall that, in [21], the spectrum was simulated by the sum of two plasma contributions with temperatures of 2000 and 600 eV. For the present experiment, the sum of two plasma contributions is also necessary, but with much lower temperatures of 600 and 100 eV (Fig. 4). Note that the above remark regarding the accuracy of the calculation of the spectral transition positions also concerns this spectral section.

The question arises as to why a plasma channel with a much lower temperature appears in this experiment, where the flux density of laser radiation was higher than that in [21]. The answer to this question is associated with the existence of the long trailing edge of the heating laser pulse, i.e., with the so-called post-

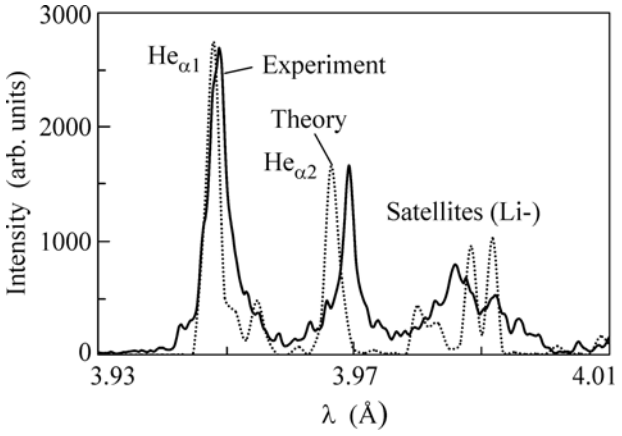


**Fig. 4.** Detected and calculated spectra for wavelength range 3.93–4.01 Å.

pulse. As was shown in [42, 43], the formation of the plasma channel is nonadiabatic and the temperature of the plasma at this stage increases due not only to the thermalization of hot electrons, but also to the heating of the plasma by the post-pulse. An increase in the contrast of the laser pulse affects only the suppression of the pre-pulse and does not affect the post-pulse. Dense plasma regions with the supercritical density in very large clusters remain to the time of the end of the main laser pulse. As a result, the post-pulse is efficiently absorbed and the temperature of the plasma increases. The efficiency of the absorption of the post-pulse in smaller clusters is lower and the heating of the plasma weakens. The lower final temperature in this experiment is confirmed by analyzing the broadband spectrum detected using the X-ray CCD (see Fig. 1c). In [21], this spectrum corresponded to an average temperature of 2000 eV, whereas in this experiment, it is well described with a temperature of 300 eV. Note that the intensity of the $He_\beta$ line at this temperature should be lower than noise; i.e., this line should be invisible, which is confirmed in this experiment.

**4.** To summarize, the reported experiments make it possible to analyze for the first time differences in X-ray emission spectra of argon clusters excited at the laser–cluster and laser–droplet interactions. The conclusions are as follows.

In contrast to the laser–droplet interaction, all parts of a cluster are heated simultaneously in the case of the laser–cluster interaction. The resulting plasma is more uniform and has a higher average temperature at this stage.

The stage of the interaction with the laser pulse makes the main contribution to the emission of the plasma in the wavelength range between $K_\alpha$ lines and *O*-like satellites. The spectra of hollow ions play the key role. Since the spectra of hollow ions are sensitive to the plasma parameters, they can be used for the plasma diagnostics at this evolution stage.

The heating of the plasma by the post-pulse is of significant importance at the stage of the formation of the plasma channel (after the end of the main laser pulse). Correspondingly, the final temperature of the plasma increases noticeably with an increase in the initial size of the cluster; this behavior ensures a more efficient absorption of the post-pulse. The spectral lines of He-like ions and their Li-like satellites can be used for the diagnostics of the parameters of the plasma channel.

This work was supported by the Russian Foundation for Basic Research (project nos. 10-02-91174-GFEN-a and 10-02-00345-a) and the Department of Energy of the United States (contract no. DE-AC52-06NA25396).

## REFERENCES

1. S. Dobosz, M. Schmidt, M. Pedrix, et al., JETP Lett. **68**, 454 (1998).
2. S. Dobosz, M. Schmidt, M. Pedrix, et al., J. Exp. Theor. Phys. **88**, 1122 (1999).
3. G. C. Junkel-Vives, J. Abdallah, Jr., F. Blasco, et al., Phys. Rev. A **64**, 021201(R) (2001).
4. A. I. Magunov, T. A. Pikuz, I. Yu. Skobelev, et al., JETP Lett. **74**, 375 (2001).
5. G. C. Junkel-Vives, J. Abdallah, Jr., F. Blasco, et al., Phys. Rev. A **66**, 033204 (2002).
6. G. C. Junkel-Vives, J. Abdallah, Jr., T. Auguste, et al., Phys. Rev. E **65**, 036410 (2002).
7. Y. Fukuda, Y. Akahane, M. Aoyama, et al., JETP Lett. **78**, 146 (2003).
8. S. B. Hansen, A. S. Shlyaptseva, A. Ya. Faenov, et al., Phys. Rev. E **66**, 046412 (2002).
9. J. Abdallah, Jr., G. C. Junkel-Vives, A. Ya. Faenov, et al., JQSRT **81**, 3 (2003).
10. N. L. Kugland, C. G. Constantin, P. Neumayer, et al., Appl. Phys. Lett. **92**, 241504 (2008).
11. N. L. Kugland, P. Neumayer, T. Doppner, et al., Rev. Sci. Instrum. **79**, 10E917 (2008).
12. A. Ya. Faenov, T. A. Pikuz, Y. Fukuda, et al., Appl. Phys. Lett. **95**, 101107 (2009).
13. A. Ya. Faenov, T. A. Pikuz, I. Fukuda, et al., JETP Lett. **89**, 485 (2009).
14. Y. Hayashi, Y. Fukuda, A. Ya. Faenov, et al., Jpn. J. Appl. Phys. **49**, 126401 (2010)
15. A. Ya. Faenov, J. Abdallah, Jr., R. E. H. Clark, et al., Proc. SPIE **3157**, 10 (1997).
16. A. M. Urnov, J. Dubau, A. Ya. Faenov, et al., JETP Lett. **67**, 513 (1998).
17. F. Liu, L.-M. Chen, X.-X. Lin, et al., Opt. Express **17**, 16379 (2009).
18. S. A. Gaillard, K. A. Flippo, M. E. Lowenstern, et al., J. Phys.: Conf. Ser. **244**, 022034 (2010).
19. L. M. Chen, F. Liu, W. M. Wang, et al., Phys. Rev. Lett. **104**, 215004 (2010).
20. U. Zastrau, A. Sengebusch, P. Audebert, et al., High Energy Density Phys. **7**, 47 (2011).

21. J. Colgan, J. Abdallah Jr., A. Ya. Faenov, et al., High Energy Density Phys. **7**, 77 (2011).
22. Y. Hayashi, A. S. Pirozhkov, M. Kando, et al., Opt. Lett. **36**, 1614 (2011).
23. C. Liu, Z. Wang, W. Li, et al., Opt. Lett. **35**, 3096 (2010).
24. A. S. Boldarev, V. A. Gasilov, and A. Ya. Faenov, Tech. Phys. **49**, 388 (2004).
25. A. S. Boldarev, V. A. Gasilov, A. Ya. Faenov, et al., Rev. Sci. Instrum. **77**, 083112 (2006).
26. A. Ya. Faenov, S. A. Pikuz, A. I. Erko, et al., Phys. Scripta **50**, 333 (1994).
27. I. Yu. Skobelev, A. Ya. Faenov, B. A. Bryunetkin, et al., JETP **81**, 692 (1995).
28. F. Blasco, C. Stenz, F. Salin, et al., Rev. Sci. Instrum. **72**, 1956 (2001).
29. J. Colgan, J. Abdallah, Jr., A. Ya. Faenov, et al., Laser Part. Beams **26**, 83 (2008).
30. J. Colgan, J. Abdallah, Jr., A. Ya. Faenov, et al., Phys. Scripta **78**, 015302 (2008).
31. A. Ya. Faenov, T. A. Pikuz, I. Yu. Skobelev, et al., J. Phys.: Conf. Ser. **163**, 012016 (2009).
32. F. B. Rosmej, A. Ya. Faenov, T. A. Pikuz, et al., J. Phys. B **32**, L107 (1999).
33. A. Ya. Faenov, A. I. Magunov, T. A. Pikuz, et al., Phys. Scripta T **80**, 536 (1999).
34. J. Abdallah, Jr., I. Yu. Skobelev, A. Ya. Faenov, et al., Quantum Electron. **30**, 694 (2000).
35. F. B. Rosmej, U. N. Funk, M. Geissel, et al., JQSRT **65**, 477 (2000).
36. I. Yu. Skobelev, A. Ya. Faenov, T. A. Pikuz, and V. E. Fortov, Usp. Fiz. Nauk 2011 (in press).
37. J. Abdallah, Jr., R. E. H. Clark, and R. D. Cowan, Los Alamos Manual No. LA 11436-M-I (1988).
38. S. Mazevet and J. Abdallah, Jr., J. Phys. B **39**, 3419 (2006).
39. R. E. H. Clark, J. Abdallah, Jr., and J. B. Mann, Astrophys. J. **381**, 597 (1991).
40. N. H. Magee, J. Abdallah, Jr., J. Colgan, et al., in *Proceedings of the 14th Topical Conference on Atomic Processes in Plasmas*, Ed. by J. S. Cohen, S. Mazevet, and D. P. Kilcrease, AIP Conf. Proc. (New York, 2004), p. 168.
41. J. Colgan, J. Abdallah, Jr., C. J. Fontes, et al., J. Phys. B **43**, 144021 (2010).
42. A. Ya. Faenov, A. I. Magunov, T. A. Pikuz, et al., JETP Lett. **86**, 178 (2007).
43. A. Ya. Faenov, A. I. Magunov, T. A. Pikuz, et al., Laser Part. Beams **26**, 69 (2008).

*Translated by R. Tyapaev*